Available online at www.sciencedirect.com
SCIENCE DIRECT
Image and Vision Computing 23 (2005) 681–691
image AND vision COMPUTING
www.elsevier.com/locate/imavis

# Fundamentals of Stop and Go active models

Oriol Pujol*, Debora Gil, Petia Radeva[1]

*Centre de Visió per Computador, Edifici O, Campus UAB, Bellaterra (Cerdanyola), Barcelona 08193, Spain*

Received 30 January 2004; received in revised form 9 November 2004; accepted 30 March 2005

**Abstract**

An efficient snake formulation should conform to the idea of picking the smoothest curve among all the shapes approximating an object of interest. In current geodesic snakes, the regularizing curvature also affects the convergence stage, hindering the latter at concave regions. In the present work, we make use of characteristic functions to define a novel geodesic formulation that decouples regularity and convergence. This term decoupling endows the snake with higher adaptability to non-convex shapes. Convergence is ensured by splitting the definition of the external force into an attractive vector field and a repulsive one. In our paper, we propose to use likelihood maps as approximation of characteristic functions of object appearance. The better efficiency and accuracy of our decoupled scheme are illustrated in the particular case of feature space-based segmentation.


*Keywords:* Deformable models; Geodesic snakes; Region-based segmentation

## 1. Introduction

Active contours ([1,3,8], to mention just a few) are well-known tools in computer vision for image segmentation [7,9,12,14] and shape recovery. These techniques interpret low-level information (i.e. edge points) under general high-level assumptions/constraints to assure well possedness of the segmentation problem. In particular, snakes are defined by internal and external constraints to deform a curve until it adapts to the object of interest. The internal constraints control continuity and smoothness of the snake, meanwhile the external ones are responsible for adjusting to the image features. In general, there are two different approaches in current snakes formulations: the parametric (physics-based) and the geometric (geodesic) definition.

Parametric deformable models [8] use Newton mechanics laws to define the internal constraints of the model. In these physical terms, such constraints are given in terms of elasticity and stretching of the snake. By working with an explicit parametrization of the curve, the model restricts the search space of the segmentation solutions to single objects. Although there are some parametric schemes [10] dealing with topological changes, they required computing a new parametrization at each iteration, resulting in time consuming algorithms. An alternative to physics-based snakes are the geodesic active contours [1]. Geodesic snakes are based on the theory of curve evolution and level sets methods [11]. In this geometric setting, the snake deforms in a Riemannian surface until its length, dependant on image features, is minimum. Its implicit level sets formulation [11] can naturally deal with topological changes during the snake evolution. This is a main advantage in those cases where the topology of the target object is not known a priori.

In most snake applications of the segmentation problem, the metric is defined based on the image gradient in order to detect edges. The geodesic snake deformation is determined by two distinct terms in its evolution equation. The first term is the normal component of the gradient of the metric and rules convergence to contours. The second one, dependant on the snake curvature, gives regularity to the snake and defines its motion at null gradient regions. That is, it also influences on the convergence scheme. The double role of the curvature term has some disadvantages: on one hand, because it is a second order term, it hinders the numeric scheme; on the other hand, it troubles snake convergence to concave areas. The usual way to overcome poor convergence to non-convex shapes is to add a constant motion term, the balloon force [3], that pushes the snake into

* Corresponding author. Tel.: +34 93 581 1828; fax: +34 93 581 1670.
*E-mail address:* oriol@cvc.uab.es (O. Pujol).
[1] Member, IEEE.

0262-8856/$ - see front matter © 2005 Elsevier B.V. All rights reserved.
doi:10.1016/j.imavis.2005.03.007

concave regions. In order to guarantee convergence into such regions, its magnitude there should be greater than the absolute value of the curvature. A major inconvenience is that the former requirement troubles stopping the snake at the desired contour. Because balloon forces correspond to a minimization of the area enclosed by the snake, they can be embedded in a region-based scheme.

Region-based methods are born to introduce region information in the geodesic formulation. They aim at finding a partition of the image such that the descriptors of each of the regions conform to a given 'homogeneity' criterion. It follows that the force guiding the snake must be derived from the competition of the descriptors. In Ronfard [17], the velocity function is proportional to the difference of simple statistical features. In Zhu [24] and Paragios and Deriche [12], the authors define the region evolution as a quotient of probabilities corresponding to different regions. In Yezzi et al. [21], a dynamical approach is defined in which the evolution of the curve is described by the difference of mean gray levels inside and outside the evolving front at each iteration. In the same way, Jehan-Besson et al. [7] propose a difference of simple statistics, variance and covariance matrix, inside and outside the curve, also recomputing that measures at each iteration. Chakraborty et al. [2] consider an evolution using a Fourier parametrization over the original image and a previously classified image regions. Most of the methods are based on simple non-supervised descriptors of image regions. This limits its applicability to segmentation of simple images. However, complex scenes such as natural and real images need more accurate descriptors for their segmentation. In this way, supervised feature extraction schemes are more suitable for the task [12,18].

Considering the general problem of region-based segmentation, we propose a new geodesic snake formulation that assures a more efficient behavior. Given that convergence and regularity are the key issues of the snake formulation, we propose a new definition where the terms ruling these properties are decoupled. As a result, the curvature term does not interfere in the convergence process but restricts its role to the shape regularity in the last stages of the snake deformation. By removing the influence of the snake curvature from the convergence step, any *global* vector field properly defining the target contour curve as its set of equilibrium points ensures convergence. However, current external forces either restrict to a band [1] (non-global) around object contours or have saddle points [22] (target curve not properly defined) that prevent the snake from entering into concave regions. We propose using the decoupling strategy for the definition of a global vector field having the target curve as the set of equilibrium points. It can be seen that any vector field fulfilling the above requirement splits into an exterior attractor vector field (GO term) and an inner repulsive one (STOP term) which sum cancels on the curve of interest. This is the milestone in the definition of our *Stop and Go* snakes: defining separately the GO and the STOP term and glue them together by means of a characteristic function. Because we want to ensure snake convergence whatever curve concavity is, a balloon force will be our GO term. Since the curvature term has been removed from the convergence step, there is no restriction on the magnitude of this force, which prevents the snake from collapsing to a point. For the STOP vector field any standard external force restricted to the object interior suffices. Its choice hinges upon the particular segmenting problem.

A mask defining the object of interest would be the ideal tool to bound the scope of the curvature term and to perform any decoupling. To address segmentation of real images, we propose to use *likelihood maps* as an approximation of the object characteristic function. A likelihood map represents the likelihood value of each pixel of the image. Since it also characterizes the object of interest we introduce its use as a STOP term. In this manner the Stop and Go scheme presented in this paper is particularly suited for feature space-based segmentation, such as textures [12,14,16], color [19,24], motion [13], etc.

Our new formulation has several advantages over current snake schemes. On one hand, except for the very last refinement steps, the technique admits arbitrary large time increments in the iterative Euler scheme used in its implementation. On the other, by removing curvature influence from the convergence process, we can build a robust vector field to be used as an external force/attraction term that ensures convergence but, at the same time, snake stabilization. The use of likelihood maps also introduces a great advantage by allowing any scheme capable to produce a likelihood map to operate in our snake framework.

The topics are addressed in the following order. Section 2 describes the background of geodesic and region-based snakes. Section 3 gives the fundamentals of the formulation of the Stop and Go snakes. Section 4 describes the *likelihood map* space as an alternative to the classic contour and mask spaces as well as the numeric issues concerning Stop and Go implementation. Section 5 discusses the experimental results and Section 6 concludes the article.

## 2. Analysis of current geometric snakes

Most of current snakes define curve evolution within an energy minimization framework. In this context, the energy functional should achieve a compromise between adjusting to image features and achieving curve regularity. There are two main tendencies for the definition of the minimizing energy.

### 2.1. Geodesic formulations in a contour space

General geodesic snake formulation defines the evolution of a snake within an energy minimization framework. In particular, the solution to the problem is the curve ($\Gamma$) of

minimum length in a Riemannian surface with a metric ($g$) depending on the image contrast changes. It follows that the snake, $\Gamma$, evolves according to

$$\frac{\partial \Gamma}{\partial t} = (g \cdot \kappa - \langle \nabla g, \vec{n} \rangle) \cdot \vec{n} \quad \text{with} \quad g = \frac{1}{1 + |\nabla u|^2} \tag{1}$$

where $\kappa$ is the curvature of $\Gamma$, $\vec{n}$ is its inward unit normal and $\langle , \rangle$ stands for the scalar product of two vectors.

We can give the following interpretation to each of the terms involved in the above formula. The term $\langle \nabla g, \vec{n} \rangle \vec{n}$ is a vector field defined on the curve pointing to the region of interest that attracts the snake to the object boundary. Since its computation essentially relies on image edges, from a vector flow point of view, it can be considered as a *Static Vector Field* locally defining the target object. The curvature term, $g \cdot \kappa \vec{n}$, influences different aspects of the snake evolution. On one hand, it defines its motion when it is located far away from the object boundaries. Since it depends on the evolving snake, it acts as a *Dynamic Vector Field* in the convergence process. On the other hand, it serves as a curve regularizing term, ensuring continuity of the final segmenting snake in a similar fashion [23] the membrane term of parametric snakes does. Finally, it gives the process a smooth behavior and ensures continuity during the deformation, in the sense that it prevents shock formation [5]. However, incorporating the curvature term into the convergence scheme has some disadvantages. First, it difficulties the snake convergence to concave areas. Second, guidance through the curvature is extremely slow, so in spite of giving regularity to the evolution equation, it hinders the numerical scheme since time increment is bounded by the second order term [20].

The main problem of (1) is that convergence to the object of interest relies on the properties of the external field. Even considering a regularization [22] of the external force, concave regions such that the unit tangent turns around more than $\pi$ between consecutive inflexion points of the object contour, can not be reached [6]. In order to increase convergence to concavities and to speed up the evolution, a constant balloon force velocity term, $V_0$, corresponding to area minimization is added:

$$\frac{\partial \Gamma}{\partial t} = (g \cdot \kappa + V_0 - \langle \nabla g, \vec{n} \rangle) \cdot \vec{n} \tag{2}$$

Notice that, in order to ensure that the scheme will stop at the boundary of interest, an equilibrium between the constant shrinking velocity, $V_0$, and the static vector field, $\nabla g$, must be achieved. One easily realizes that, should this condition be satisfied, incorporating the curvature term into the convergence scheme constitutes a significant drawback. For $V_0$ must overpass the magnitude of $\kappa$ to enter into concave regions but, at the same time, it should be kept under $\min|\langle \nabla g, \vec{n} \rangle|$ (minimum taken on the curve to detect!) to guarantee non-trivial steady states. This dichotomy motivates the bounding the scope of $V_0$ to a given image region [7].

### 2.2. Snake formulation in a region scheme

The 'region terms' [7] are added to the minimization scheme as follows:

$$E(\Omega_{\text{in}}, \Omega_{\text{out}}, \Gamma) = \int\int_{\Omega_{\text{in}}} g^{(\Omega_{\text{in}})} \mathrm{d}x\mathrm{d}y + \int\int_{\Omega_{\text{out}}} g^{(\Omega_{\text{out}})} \mathrm{d}x\mathrm{d}y + \int_{\Gamma} g^{(\Gamma)} \mathrm{d}s$$

where $\Omega_{\text{in}}$ and $\Omega_{\text{out}}$ refer to the inside and outside of the region of interest. There are two different approaches to determine the region: a 'pseudo-static' approach and a dynamic one. In the first case, the attraction term that guides the evolution of each point in the curve is previously computed and kept fixed during the evolution [12,24]. In the second one, measures of the regions descriptors depend on the evolving curve [2,21], so that all parameters must be updated at each iteration.

Region-based approaches usually rely on a pseudo-mask behavior [24], which can be implemented by considering:

$$M(x, y) = \begin{cases} \alpha & \text{if } P_{\text{Background}} > P_{\text{Target}} \\ -\alpha & \text{otherwise} \end{cases}$$

and evolving the snake using:

$$\frac{\partial \Gamma}{\partial t} = \text{sign}(I) \cdot \vec{n} \tag{3}$$

We propose to reformulate (2) decoupling the regularity and convergence terms and embedding the scheme in a region-based framework.

## 3. Stop and Go snakes

Putting aside the energy minimization interpretation, the evolution of the curve is basically guided by an external force which defines an equilibrium state of the evolution. Whatever the external vector field, from the point of view of the evolving curve, achieving an equilibrium state can be decoupled into two stages: a straight forward advancing front defined outside the region of interest, and an inside region term opposed to it. Evolution stops if these two forces cancel along the curve of interest. Standard snake vector fields will serve to build an external force ensuring convergence and a mask of the region of interest, $I$, will be used to perform any vector decoupling/restriction.

### 3.1. Basics of Stop and Go formulation

In any minimization process, the snake deforms under two different vector flows: an attractor vector field (GO) moving the curve towards the target and a repulsive one (STOP) making that evolution stop. By means of

the characteristic function of the region of interest, namely $R$:

$$I(x,y) = \begin{cases} 1 & \text{if } (x,y) \in R \\ 0 & \text{otherwise} \end{cases}$$

these two motions can be decoupled. Let us assume once again that the evolving curve is outside the region of interest. Then, in a region-based approach, the GO term corresponds to an area minimization process restricted to the outside of $R$:

$$V_{\mathrm{GO}} = (1 - I) \cdot V_0 \cdot \vec{n} \tag{4}$$

The above equation creates a dynamic 'inward' motion to the region of interest, in the same fashion of that of 'balloon' snakes. In order to define the outward 'motion', notice that there is no need to define the STOP field on the whole image. The scheme will work, as long as this vector is well defined in the environment of the contour we are looking for. Therefore, the STOP term can be defined by the 'outward' gradient of any function, namely $g$, locally defining the contours of the object of interest:

$$V_{\mathrm{STOP}} = I \cdot \langle \nabla g, \vec{n} \rangle \vec{n} \tag{5}$$

It follows that the evolution of an outward initial curve to the region of interest in Stop and Go formulation is given in the following terms:

$$\frac{\partial \Gamma}{\partial t} = \underbrace{\langle I \cdot \nabla g, \vec{n} \rangle \vec{n}}_{\text{Stop}} + \underbrace{V_0 \cdot (1 - I) \cdot \vec{n}}_{\text{Go}} \tag{6}$$

As in the case of balloon snakes, the sum of both terms defines an (oscillating) equilibrium solution if we assure that $V_0 + \langle \nabla g, \vec{n} \rangle \leq 0$ on the boundary of $R$. The fact that the term $V_0(1 - I) \cdot \vec{n}$ comes from an area minimization process has the following effects. First of all, by varying the $V_0$ parameter we will be able to ignore sparse responses of the potential $g$ of small area, such as spurious noise. Second, it can swallow low valued areas of the potential.

The drawings in Fig. 1 illustrate the grounds of a Stop and Go field. A standard static field, $\nabla g$, having the circle as minimum is displayed in Fig. 1(a). Its decomposition into the repulsive, $I \cdot \nabla g$ and attractive, $(1 - I) \cdot \nabla g$, vector fields is shown, respectively, in Fig. 1(b) and (c). We observe that, like in any geodesic formulation, the $V_{\mathrm{STOP}}$ term given by formula (5) corresponds to the projection of the repulsive vector field onto the snake unit normal, $\vec{n}$. Finally, Fig. 1(d) represents a dynamic $V_{\mathrm{GO}}$ field for the case of a shrinking ellipse placed outside the target gray circle.

### 3.2. Improving Stop and Go with a regularizing term

The 'Stop and Go' approach leads a curve to the desired boundary, however some smoothness and continuity is desired on the final model. Because regularity is only necessary in the final steps of the snake deformation, we will bound its scope to a neighborhood of the target object. Such restriction can be performed by means of a smoothed version of the mask $\check{I} = G_\sigma * I$; for $G_\sigma$ a gaussian filter with standard deviation $\sigma$. Adding this regularity term to (6) the final evolution equation of Stop and Go snakes yields:

$$\Gamma_t = \underbrace{(I\langle \nabla g, \vec{n} \rangle + V_0(1 - I)) \cdot \vec{n}}_{\text{Stop and Go}} + \underbrace{\alpha \kappa \check{I} \vec{n}}_{\text{Reg. term}} \tag{7}$$

The above formulation can be interpreted as selecting among all curves approaching the boundary of the target object, those complying to a given degree of regularity. Hence our formulation highly resembles that of parametric snakes, in the sense that regularity and convergence have been decoupled.

Reducing the action range of the regularizing term, endows curvature with a radically different role than it had in geodesic snakes. Firstly, it is a strictly regularizing term (like parametric snakes internal energy), which easies controlling its importance on the final curve by means of the weighting $\alpha$. Secondly, since its scope is bounded to the last steps of the snake deformation, it does not trouble convergence to the contour concave regions. Finally, by restricting curvature to a band around contours, the integration step in an Euler numeric scheme, related to second order terms [5], is not a critical value. It follows that, except for the very last refinement steps, it can be arbitrarily high, so that speed of convergence increases. The above comments makes the scheme given by (7) conform to the following naive idea: obtaining a rough representation of objects should be computationally efficient, only requiring regularity is computationally expensive.

An important remark on the regularity of the final curve should be made. It is well known that the curvature term

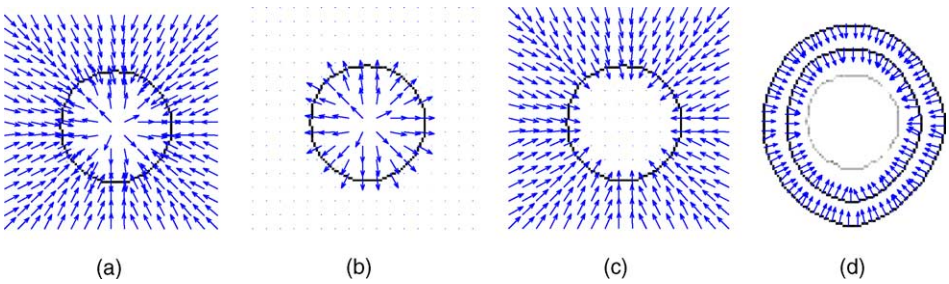


Fig. 1. External force decoupling into Stop and Go terms. (a) Static external force. (b) Repulsive term. (c) Attractive term. (d) Dynamic go term.

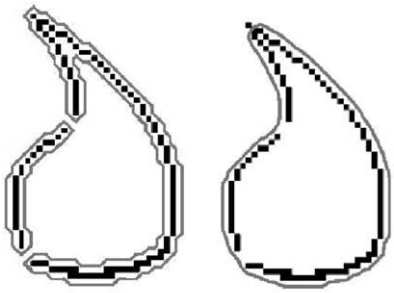


Fig. 2. Open drop. (a) Snake without regularity term and (b) Stop and Go snake.

alone only guaranties continuity of the curve, preventing the snake from leaking into small holes. However, our scheme takes advantage of a synergy between the Stop and Go formulation and the curvature term to introduce a higher smoothness in the final shape. If we reformulate (7) as:

$$\frac{\partial \Gamma}{\partial t} = \underbrace{(V_0 + I\langle \nabla g, \vec{n}\rangle)\vec{n}}_{\text{Convergence}} + \underbrace{I\bullet(\alpha\kappa - V_0)\vec{n}}_{\text{Regularizing term}}$$

we find that, if a small $V_0$ ensures convergence, the snake regularity follows from the competition between curvature and $V_0$ near the object boundary. We argue that such competition yields our model a smoothness close to that of parametric snakes. Note that there is a substantial difference in geodesic schemes, which both terms contribute in the convergence stage and only curvature affects in the snake regularity.

Fig. 2 illustrates the effect of the competition between $V_0$ and curvature. The Stop and Go active model is shown deforming over a contour map, thus serving as an illustration of its usage in this kind of space. Fig. 2(a) shows the final snake obtained without the regularizing term and Fig. 2(b) the result of adding it. As in geodesic snakes, the curvature prevents the snake from leaking through small holes yielding a closed model of the drop. But, notice that the curve in Fig. 2(b) is smoother than the linear geodesic interpolation.

## 4. Stop and Go snakes design

### 4.1. Term decoupling

Lacking of object masks in practical applications motivates searching for an alternate to perform the decoupling needed in the Stop and Go snakes. In the general case, any map defining the object to detect as a local extremum (minimum or maximum) and taking negligible values outside the environs of the object would serve. For instance, the response of the image to a bank of filters or characterizing features are suitable maps. In this paper, we will consider likelihood maps as an approximation of object masks.

The likelihood map is defined as the likelihood value for each of the pixels of a given space to represent the target object. We can think of likelihood values as pseudo-probabilities, which represent a continuous pseudo-density function. Likelihood maps contain information about the accuracy of the classification to avoid false positive classified regions. This solves the deficiencies of the classic region approaches, which use heuristically defined vector fields to create the velocity term of the snake. Usually, these approaches need previous classifications or contain implicit classification schemes, on which there is little control over the false positive and false negative regions unless some (regularizing) region term ([12], Zhu [24]) is added.

Our likelihood map is computed by means of the following standard approach [4]. We adjust a mixture of gaussian to the values describing textures in the feature space (probability density function estimation). The mixture of gaussians is given by:

$$MG(x, \Theta) = \sum_{r=1}^{k} \alpha_r G_{\mu_r,\sigma_r}(x)$$

where $G_{\mu_r,\sigma_r}(x)$ is a gaussian density function, $k$ is the number of gaussians involved, $\Theta = (\mu_1,\ldots,\mu_k, \sigma_1,\ldots,\sigma_k)$ are the gaussians' mean values and standard deviation matrices. The model is adjust using an expectation maximization procedure [4]. Unfortunately, the former standard way of computing the likelihood map has as a main drawback its lack of accuracy at the real boundaries of the region of interest. To be precise, the set of regions with high likelihood value representing the objects of interest are smaller in size than the true objects. We improve its accuracy by using a two-class enhancing procedure or a sharpening using connected components with max-trees ([14,15]) in order to topologically enhance contours.

In Fig. 3(b)–(d), different likelihood maps for the textured tetra-foil of Fig. 3(a) are shown. The standard likelihood map resulting from the mixture model is displayed in Fig. 3(b). Finally, Fig. 3(c) shows the enhanced likelihood map using the two-class enhancing procedure. As one can see, the borders are better defined and some low likelihood areas which belong to the tetra-foil region are emphasized. Fig. 3(d) shows the result after the topological enhancement. We can observe that the borders are clearly defined and the low likelihood regions are further emphasized keeping the general topology of the tetra-foil unchanged. Therefore, our estimation of the object mask will be a version of the likelihood map, $\check{L}$, normalized between 0 and 1. That is, replacing $I$ by $\check{L}$ in the Stop and Go formulation proposed in Section 3, we obtain the following evolution equation:

$$\frac{\partial \Gamma}{\partial t} = \alpha\kappa\check{L}\bullet\vec{n} + \check{L}\langle \nabla g, \vec{n}\rangle\bullet\vec{n} + V_0(1 - \check{L})\bullet\vec{n}$$

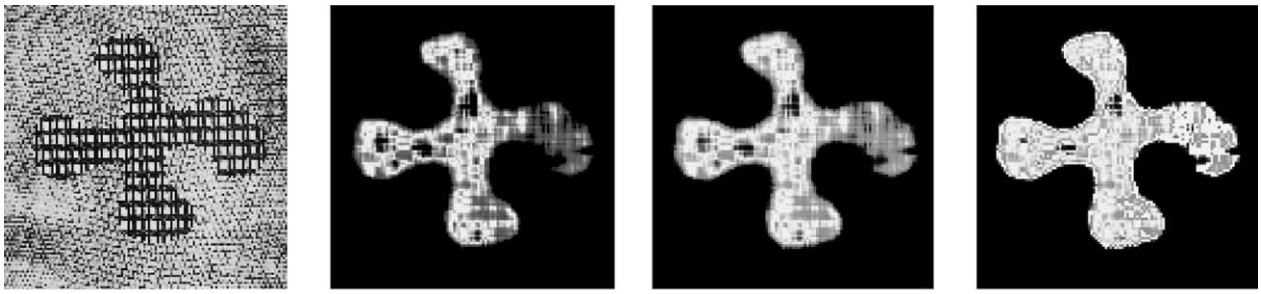


Fig. 3. Different likelihood map enhancements. (a) Original image. (b) Likelihood map associated to the tetra-foil figure texture. (c) Two class enhancing result of the likelihood map. (d) Topological enhanced likelihood map.

It only remains to define the STOP term, $\breve{L}\cdot\nabla g$, that defines the object of interest.

### 4.2. Using likelihood maps to define the Stop and Go field

The choice of the function $g$ depends on the particular segmenting problem we handle. In a contour-based space setting, the object of interest is defined by image contrast changes, meanwhile, likelihood maps are more suitable in the case of more complex features (such as, statistical, texture-based, motion-based, color-based, etc.). We propose basing the STOP term on likelihood maps for feature spaces-based segmentation and define the STOP term as $\nabla(1-\breve{L})$. Besides, since the former gradient is negligible outside a band around contours, we can merge the two STOP factors and use:

$$\frac{\partial \Gamma}{\partial t} = \alpha\kappa\breve{L}\cdot\vec{n} + \beta\langle\nabla(1-\breve{L}),\vec{n}\rangle\cdot\vec{n} + V_0(1-\breve{L})\cdot\vec{n} \tag{8}$$

### 4.3. Stop and Go numeric formulation

Evolution of an initial snake $\Gamma_0$ under (8) is implemented using the Level Sets [11] formulation. That is, given any initial surface ($\phi_0$) properly defining the interior of $\Gamma_0$, the snake evolution at time $t$ coincides with the 0 level contour of the solution to:

$$\frac{\partial \phi}{\partial t} = \left(\alpha\breve{L}\,\mathrm{div}\left(\frac{\nabla\phi}{|\nabla\phi|}\right) + V_0(1-\breve{L})\right)|\nabla\phi| + \langle\nabla(1-\breve{L}),\nabla\phi\rangle$$

The explicit Euler scheme we use in the numeric implementation of the former equation is given by:

$$\begin{aligned}\phi_{t+1} =& \phi_t + \left(\alpha\breve{L}\frac{u_{xx}u_y^2 - 2u_{xy}u_xu_y + u_{yy}u_x^2}{|\nabla u|^2}\right.\\ &\left. + V_0(1-\breve{L})|\nabla\phi_t| + \langle\nabla(1-\breve{L}),\nabla\phi_t\rangle\right)\Delta t\end{aligned} \tag{9}$$

where $\phi_t$ stands for the solution at time $t$ and derivatives are computed using centered finite differences. Notice that the speed of convergence hinges upon the magnitude of the time step $\Delta t$, the higher it is, the less iterations the algorithm needs. Accuracy is determined by $V_0$.

## 5. Stop and Go performance

We have split experimental assessment of Stop and Go performance into two blocks. First, a comparison to other geometric snakes is carried out; second, we show robustness of our formulation to the critical parameters, $\Delta t$ and $V_0$. The methodology of comparison we have used is as follows.

### 5.1. Experimental setting

We have compared our approach with a standard geodesic (2) and region-based (3) approaches. For the region-based approach we have used a thresholded version of the estimated characteristic function and for geodesic snakes its edges. All methods have been implemented using an explicit Euler scheme and initial snakes located at the frame of the image.

Experiments focus on determining snake efficiency in terms of accuracy and speed of convergence. These quantities will be measured as follows:

- Snake accuracy is given by the maximum and mean distances to the target curve. Maximum distances is the measure that best detects failure to enter into concave regions.
- Speed of convergence corresponds to the number of iterations necessary to stabilize the snake. We recall that in an explicit Euler scheme, the number of iterations is proportional to the time step, $\Delta t$, used.

### 5.2. Comparison results

We have tested the different methods on the tetra-foil (Fig. 4) and a highly non-convex shape (Fig. 6); the first shape to assess accuracy and regularity of the methods and the second one their convergence. In all cases, parameters are chosen so that the algorithms reach their optimal

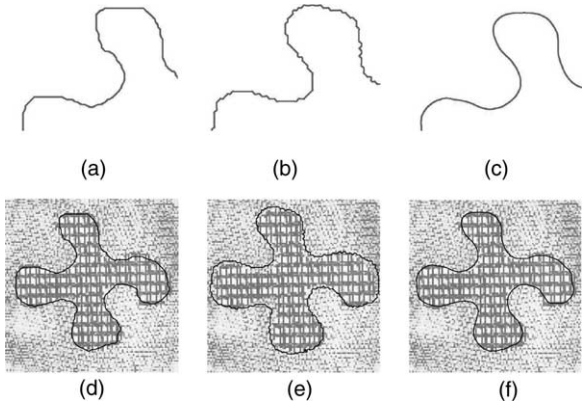


Fig. 4. Segmentation of the tetra-foil. Details of (a) geodesic, (c) region-based and (e) *Stop and Go* snakes. Segmented images for (b) geodesic, (d) region-based and (f) *Stop and Go* snakes.

performance rate in terms of achieving the best compromise between convergence to the boundary of interest, stabilization and computational time.

In the case of the tetra-foil (Fig. 4), the parameters used for geodesic snakes are $\{V_0=0.6,\ \Delta t=0.2\}$. The balloon force value is the maximum admitted by the algorithm in order to converge to the concave area and not collapsing to a point. The integration step is the higher admissible for a stable algorithm, although this jeopardizes the final curve regularity (see detail in Fig. 4(a)). For the region-based snakes $\Delta t=100$, so that speed of convergence is optimized. Stop and Go snakes use their standard configuration $\{V_0\in[0.3,1],\ \Delta t=1,\ \alpha=0.35\}$, which guarantees the best compromise between speed of convergence and accuracy.

The final segmentations are drawn in Fig. 4, the first row showing a close up of the resulting snakes captures the visual differences among the techniques. The regularity endowed by curvature makes the standard geodesic segmentation (Fig. 4(a) and (b)) smoother than the oscillating contour given by the region-based approach (Fig. 4(c) and (d)). We could get a smoother (though piecewise linear) geodesic model if the integration step was decreased, although this would decrease the speed of convergence. In the case of region-based methods, they always converge to wavy shapes by their own design, since the final approximation only depends on the shape of the object of interest and displays all the details without smoothing. By its design, Stop and Go (Fig. 4(e) and (f)) searches for a compromise between minimum length and maximum area yielding smoother final results.

Plots in Fig. 5 of the mean and maximum distances during the evolution reflect snake efficiency and its evolution smoothness. Smooth motion in the last steps is crucial to stabilize the snake at the equilibrium curve as oscillations in its energy trouble any standard stop criterion. Solid line graphics in Fig. 5 correspond to Stop and Go, dotted ones to geodesic snakes and dashed ones to region-based snakes. The ordinate axes are the distances in pixels and the abscise axes the number of iterations, mean distances are in the first row and maximums in the second one. In Fig. 5(b) and (d), we display close ups of the last

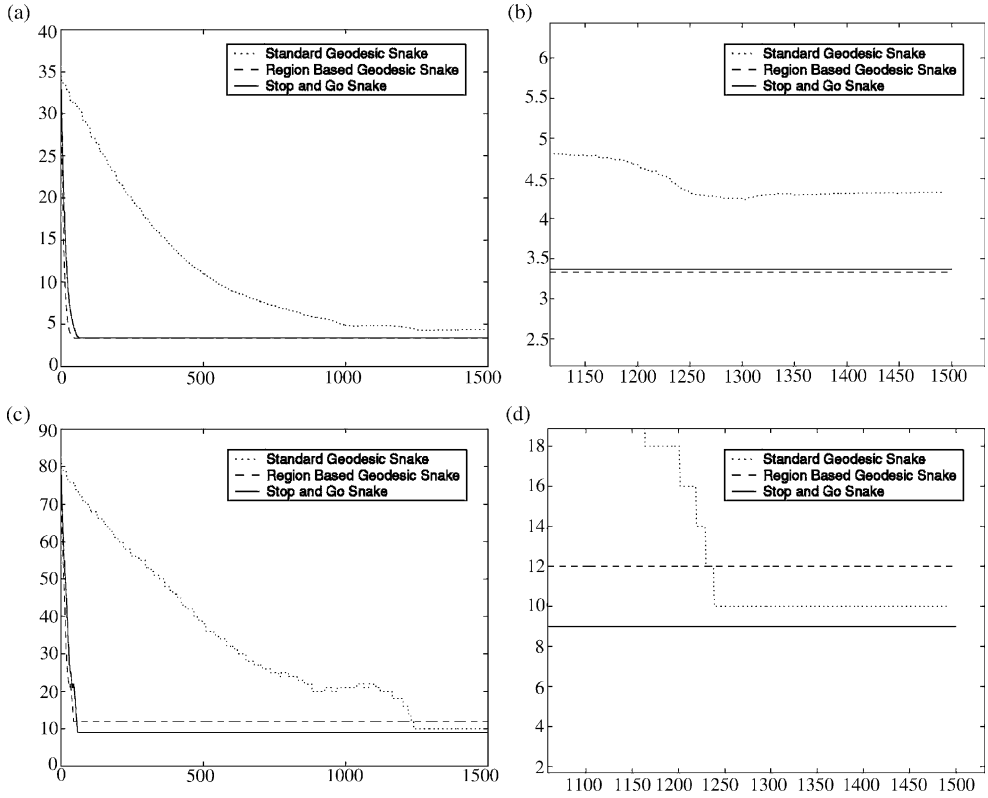


Fig. 5. Efficiency assessment for the tetra-foil. Mean distance plot (a) and (b) detail. Maximum distance (c) and detail of the last steps of the evolution (d).

iterations of the convergence process. Concerning speed of convergence, Stop and Go standard configuration compares to region-based methods for both mean (Fig. 5(a)) and maximum distances (Fig. 5(c)). Meanwhile, in spite of using their optimal speed configuration, geodesic snakes are, by no means, the worst performers. That is a consequence of the curvature term that requires a small time step and hinders entering into concave areas. Maximum distances are similar for all techniques with a difference of $<4$ pixels (see detail of Fig. 5(d)), which reflects the good convergence of all three techniques. The hill in the geodesic snake maximum distance (Fig. 5(c)) corresponds to its entrance into the tetra-foil concave segments. This phenomenon is produced by ridges in the Euclidean distance map and is common to all methods. However, because Stop and Go and region-based snakes convergence scheme lacks of the curvature term, they easily overpass concavities, so that this convergence phase is hardly detected in their maximum distance graphics.

In the case of the bracelet (Fig. 6), geodesic snakes used $\{V_0=0.6, \Delta t=0.2\}$ for Fig. 6(c) and $\{V_0=1.3, \Delta t=0.2\}$ for Fig. 6(c). The first parameter setting is the tetra-foil one. The second one is the minimum value that allows the snake to surpass the saddle point that impedes the snake to converge in the concave region. Again region-based snakes have been implemented using the highest time increment possible, $\Delta t=100$, and Stop and Go its standard configuration $\{V_0\in[0.3,1],\ \Delta t=1,\ \alpha=0.35\}$. Notice the robustness in parameter setting of the last two techniques, which converge (Fig. 6(a) and (b)) with standard values. Geodesic snake performance significantly differs. On one hand, with the tetra-foil configuration, geodesic snakes fail to converge to the right shape (Fig. 6(c)). On the other, with the higher balloon force parameter setting they collapse to a point (Fig. 6(d)).

### 5.3. Stop and Go parameters study

In order to check robustness of final models to parametric values, we have chosen the tetra-foil image (Fig. 4). The experiment consists in varying separately each of the parameters, while keeping the rest within their standard range of values. Performance is assessed by studying quality plots (Fig. 7).

Fig. 7(a) shows Stop and Go behavior when the time step varies. As expected the speed of convergence increases as $\Delta t$ raises. The time step can be increased without altering the accuracy performance provided that $\Delta t\cdot\alpha\leq 0.4$. The latter constrain is required at the last steps, when the curvature shows. Fig. 7(b) depicts the result of altering $V_0$ keeping $\Delta t=1$. To avoid the snake collapsing to a point, we should keep $V_0$ below 1.7, so that the GO term does not exceed the STOP term. Again, the convergence rate increases as the value of $V_0$ does. However, in this case, accuracy is affected as detail in Fig. 7(c) shows. The accuracy improvement for low $V_0$ is due to the fact that likelihood maps usually underestimate the object of interest. Fig. 7(d) and (e) show optimal configurations (for accuracy and speed of convergence) of the Stop and Go scheme compared to the standard one. The fastest configuration uses $\{V_0=1.3,\ \Delta t=1.3$ and $\alpha=0.23\}$ and the smoother $\{V_0=0.2, \Delta t=0.5$ and $\alpha=0.6\}$. If $V_0$ is comparable to $\kappa\cdot\alpha$ and $\Delta t$ is low, the competition between both terms allows smoother behaviors. This follows because the number of iterations, which the competition between area maximization and minimum length takes place, is larger.

The difference in behaviors consequence of the wide range of parametric values results in some interesting applications. In some cases the shape we are looking for is ambiguous, in the sense that multiple interpretations can be offered for the same shape, as, for example, the wheel-shaped image in Fig. 8. Depending on our application, we would rather have a closed round contour or an model of the open contour. This kind of control on the evolving snake can be achieved by varying the parameter $V_0$. Fig. 8(a) shows the Stop and Go snake leaking through the hole to adapt explicitly to the shape. Fig. 8(b) illustrates the effect of reducing $V_0$ if our desire is to close the hole in the shape.

### 5.4. Application to real scenes segmentation

This section provides visual validation of the Stop and Go scheme applied to real scene (textured-based) segmentation and robustness to different likelihood maps computation.

Fig. 9(a) shows the likelihood map of the zebra pattern and Fig. 9(b) shows the final segmentation using Stop and Go active models. Note the fact that the shadow of the zebra has lower probabilities than the rest. The Stop and Go active model ignores areas of a low likelihood value that would trap snakes evolving under other schemes. Notice that the shadow under the rear legs of the zebra is intense,

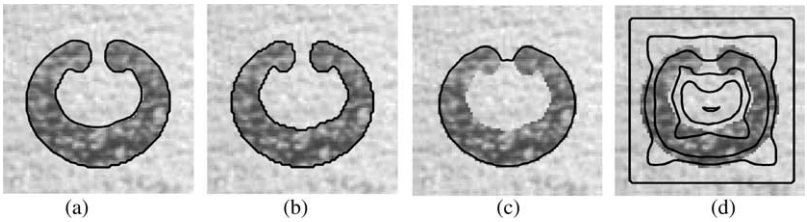


Fig. 6. Segmentation of the bracelet. (a) Stop and Go, (b) region-based snakes, (c) non-convergent geodesic snake and (d) collapsing of a geodesic snake.

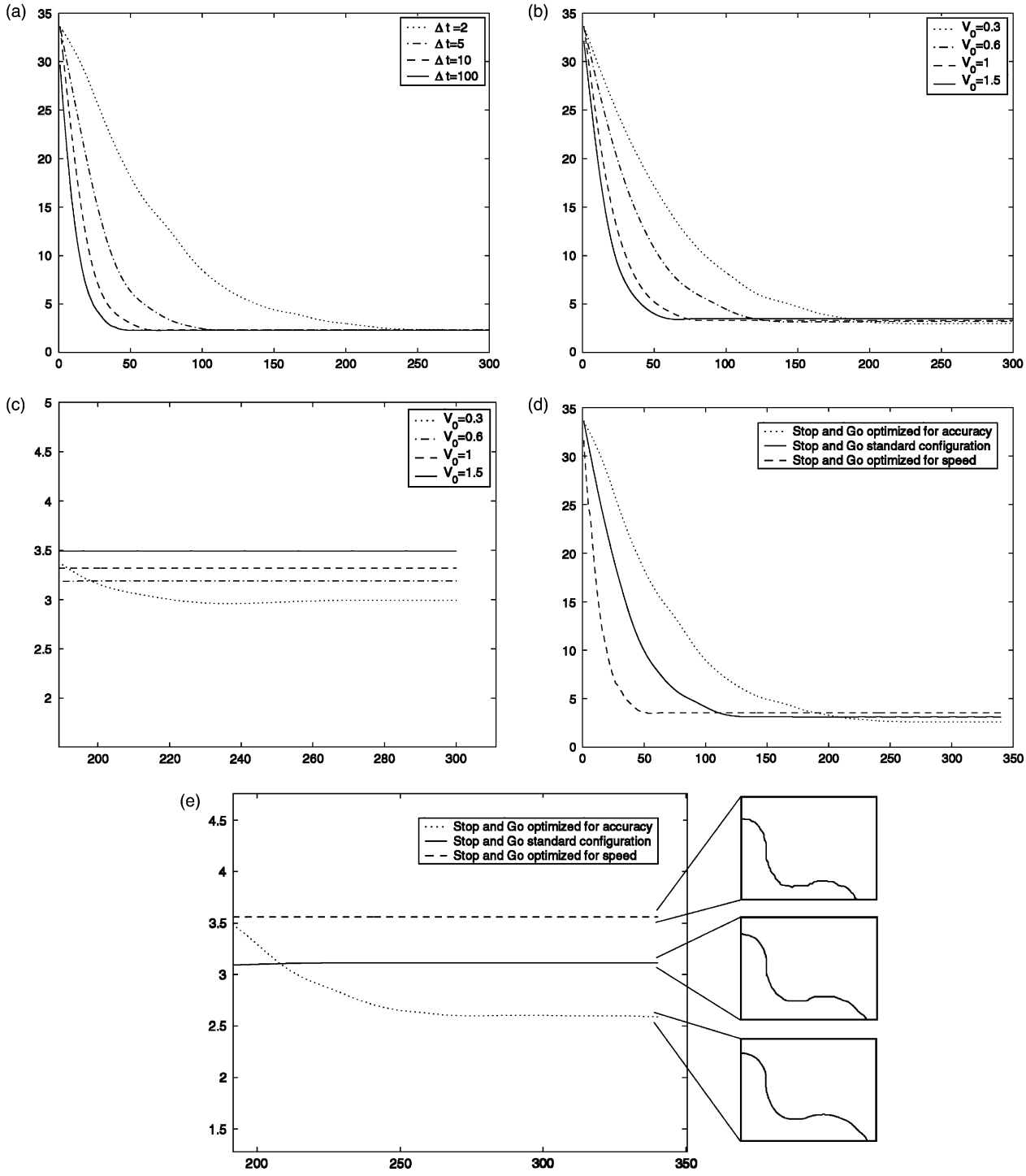


Fig. 7. *Stop and Go* parameters study. Distances for (a) time increment variation, (b) $V_0$ variation and (d) optimal parameters. Details for (c) $V_0$ plot and (e) optimal parameters plot.

and the likelihood value at that area is high. Therefore, unless we change the likelihood map the rear legs will not be segmented. Fig. 9(c) shows the likelihood map of a salamander texture applied over image (Fig. 9(d)). The background yields a large amount of false positive regions that does not correspond to the salamander. Because they have a low likelihood value, they do not affect Stop and Go behavior. The former control of the snake on low likelihood valued areas is one of the advantages of the method when used on real scenarios.

In order to illustrate robustness to likelihood map estimation, as well as, the effect of varying $V_0$ in real scenes we have chosen the tiger in Fig. 10. In this case, the likelihood map (Fig. 10(a)) computation has derived from a

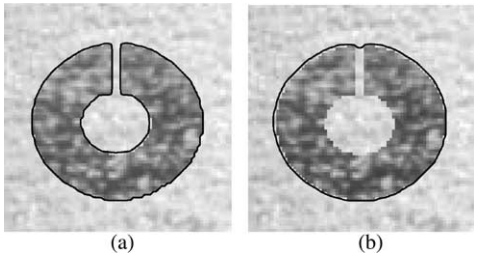

Fig. 8. Segmentation of ambiguous image using *Stop and Go* snakes. (a) Concave contour and (b) convex closure.

pseudo-naive Bayes approach [4]. The high amount of background noise would difficult the convergence of a standard snake scheme that would produce a result similar to the lowest $V_0$ in Fig. 10(b). However, our snakes admit values for the balloon force as large as to successfully cope with noise (Fig. 10(c))

## 6. Conclusion

In this paper, we have introduced a new geodesic snake model Stop and Go for a more efficient convergence to shapes. The formulation bases on restricting the regularizing term to the last stages of the snake deformation by decoupling the convergence from the regularity. This decoupling has several advantages over existent geodesic formulations. On one hand, the numeric scheme is more efficient since it admits arbitrary large time increments, except for the last regularizing steps. On the other hand, we build a robust vector field ensuring convergence but, at the same time, snake stabilization. Convergence is achieved by defining separately a dynamic attractive term and an image feature-based repulsive one. We also introduce likelihood maps to decouple as well as to define the STOP term of the external potential vector field. By using likelihood maps as an external force the particular version of Stop and Go presented in the paper is suited for feature space-based image segmentation (texture, motion, color schemes).

We have compared our scheme to current geometric snakes in terms of computational efficiency and accuracy. The results clearly show that our method outperforms geodesic snakes in terms of speed of convergence and adaptability to concave regions. Besides, the final models of shapes obtained are smoother than the ones that simple region-based scheme yields. Results on real images illustrate the applicability of likelihood maps in different feature spaces.

We are currently working on likelihood map enhancements for a better location of boundaries in natural scenes as well as on a general mathematical framework for the model. The former issues will be presented in a future work, also including an exhaustive comparison of the performance of Stop and Go snakes to the most popular texture and color-based techniques.

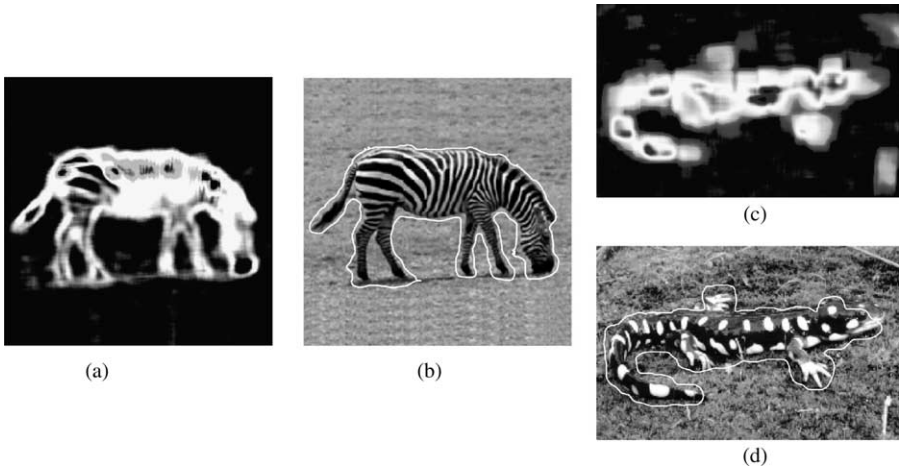

Fig. 9. Zebra segmentation: (a) Likelihood map and (b) *Stop and Go*. Salamander segmentation: (c) likelihood map and (d) *Stop and Go*.

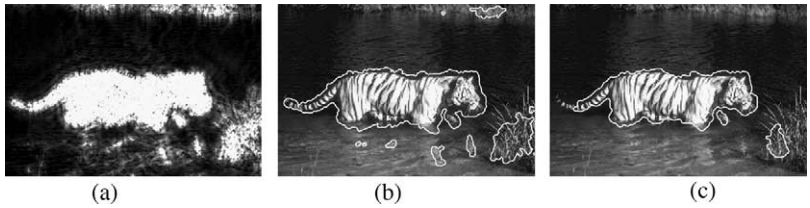

Fig. 10. Tiger image: (a) likelihood map using pseudo-naive Bayes and (b), (c) snakes for different $V_0$s.

## Acknowledgements

This work was partially supported by the project TIC2000-1635-C04-04 of CICYT, Ministerio de Ciencia y Tecnología of Spain.

## References

[1] V. Caselles, F. Catte, T. Coll, F. Dibos, A geometric model for actives contours, Numerische Mathematik 66 (1993) 1–31.
[2] A. Chakraborty, L. Staib, J. Duncan, Deformable boundary finding in medical images by integrating gradient and region information, IEEE Trans. Med. Imaging 15 (1996) 859–870.
[3] L.D. Cohen, On active contour models and ballons, CVGIP: Image Understanding 53 (2) (1991) 211–218.
[4] R. Duda, P. Hart, Pattern Classification, second ed., Wiley-Interscience, New York, 2001.
[5] L.C. Evans, Partial Differential Equations, Berkeley Mathematics Lecture Notes, vol. 3B 1993.
[6] D. Gil, P. Radeva, Curvature Vector Flow to Assure Convergent Deformable Models. EMMCVP'03, 2003.
[7] S. Jehan-Besson, M. Barlaud, G. Aubert, DREAM 2 S: deformable regions driven by an eulerian accurate minimization method for image and video segmentation, IJCV 53(1) (2003) 45–70.
[8] M. Kass, A. Witkin, D. Terzopoulos, Snakes, active contour models, Int. J. Comput. Vis. 1 (4) (1987) 321–331.
[9] T. McInerney, D. Terzopoulos, Deformable models in medical images analysis: a survey, Med. Image Anal. 1 (2) (1996) 91–108.
[10] T. McInerney, D. Terzopoulos, T-snakes: topology adaptative snakes, Med. Image Anal. 4 (2000) 73–91.
[11] S. Osher, J.A. Sethian, Fronts propagating with curvature-dependent speed: algorithms based on Hamilton-Jacobi formulations, J. Comp. Phys. 79 (1988) 12–49.
[12] N. Paragios, R. Deriche, Geodesic active contours for supervised texture segmentation, Proc. Comput. Vis. Pattern Recogn. 2 (1999) 422–427.
[13] N. Paragios, R. Deriche, Unifying boundary and region-based information for geodesic active tracking, Proc. Comput. Vis. Pattern Recogn. 2 (1999) 300–305.
[14] O. Pujol, P. Radeva, Texture segmentation by statistical deformable models, Int. J. of Img. Graphi. 4(3) (2004) 433–452.
[15] Oriol. Pujol, A Semi-Supervised Statistical Framework and Generative Snakes for IVUS Analysis. PhD thesis, Nov. 2004.
[16] T. Hofmann, J. Puzicha, J.M. Buhmann, Unsupervised texture segmentation in a deterministic annealing framework, IEEE Trans. Pattern Anal. Mach. Intell. 20 (8) (1998) 803–818.
[17] R. Ronfard, Region-based strategies for active contour models, Int. J. Comput. Vis. 13 (2) (1994) 229–251.
[18] C. Samson, L. Blanc-Féraud, G. Aubert, J. Zerubia, A level set model for image classification, Proc. Scale-Space Theor. Comp. Vis. (1999) 26–27.
[19] G. Sapiro, Color snakes, Comput. Vis. Image Understanding 68 (2) (1997) 247–253.
[20] A. Tveito, R. Winther, Introduction to partial differential equations, Texts in applied mathematics, vol. 29, Springer, New York, 1998.
[21] A. Yezzi, A. Tsai, A. Willsky, A Statistical Approach to Snakes for Bimodal and Trimodal Imagery, International Conference on Image Processing, Kobe, Japan, 1999.
[22] C. Xu, J.L. Prince, Generalized gradient vector flow external forces for active contours, Signal Process., Int. J. 71 (2) (1998) 132–139.
[23] C. Xu, A. Yezzi, J. Prince, On the Relationship between Parametric and Geometric Active Contours, Proceedings of 34th Asilomar Conference on Signals, Systems, and Computers, 2000 pp. 483–489.
[24] S.C. Zhu, Region Competition: Unifying Snakes, Region Growing, and Bayes/MDL for Multi-band Image Segmentation. Harwad Robotics Laboratory, Technical Report 94-10.